uicc
global cancer control

IJC
International Journal of Cancer

The selective VEGFR1-3 inhibitor axitinib (AG-013736) shows antitumor activity in human neuroblastoma xenografts

Jochen Rössler[1,2], Yann Monnet[1], Francoise Farace[3], Paule Opolon[4], Estelle Daudigeos-Dubus[1], Abderrahmane Bourredjem[5], Gilles Vassal[1] and Birgit Geoerger[1]

[1] UPRES EA 3535, Pharmacology and New Anticancer Treatments, University Paris-Sud, Institut Gustave Roussy, Villejuif, France
[2] Division of Pediatric Hematology and Oncology, University Hospital of Freiburg, Freiburg/Breisgau, Germany
[3] Translational Research Laboratory, Inserm U981, Institut Gustave Roussy, Villejuif, France
[4] UMR8121 Vectorology and Gene Transfer, Institut Gustave Roussy, Villejuif, France
[5] Biostatistics and Epidemiology Unit, Institut Gustave Roussy, Villejuif, France

Tumor angiogenesis in childhood neuroblastoma is an important prognostic factor suggesting a potential role for antiangiogenic agents in the treatment of high-risk disease. Within the KidsCancerKinome project, we evaluated the new oral selective pan-VEGFR tyrosine kinase inhibitor axitinib (AG-013736) against neuroblastoma cell lines and the subcutaneous and orthotopic xenograft model IGR-N91 derived from a primary bone marrow metastasis. Axitinib reduced cell proliferation in a dose-dependent manner with IC_{50} doses between 274 and >10,000 nmol/l. Oral treatment with 30 mg/kg BID for 2 weeks in advanced tumors yielded significant tumor growth delay, with a median time to reach five times initial tumor volume of 11.4 days compared to controls ($p = 0.0006$) and resulted in significant reduction in bioluminescence. Simultaneous inhibition of VEGFR downstream effector mTOR using rapamycin 20 mg/kg q2d×5 did not statistically enhance tumor growth delay compared to single agent activities. Axitinib downregulated VEGFR-2 phosphorylation resulting in significantly decreased microvessel density (MVD) and overall surface fraction of tumor vessels (OSFV) in all xenografts as measured by CD34 immunohistochemical staining (mean MVD ± SD and OSFV at 14 days 21.27 ± 10.03 in treated tumors *vs.* 48.79 ± 17.27 in controls and 0.56% *vs.* 1.29%; $p = 0.0006$, respectively). We further explored the effects of axitinib on circulating mature endothelial cells (CECs) and endothelial progenitor cells (CEPs) measured by flow cytometry. While only transient modification was observed for CECs, CEP counts were significantly reduced during and up to 14 days after end of treatment. Axitinib has potent antiangiogenic properties that may warrant further evaluation in neuroblastoma.

Neuroblastoma is the most frequent extra cranial solid tumor of early childhood. It shows extremely variable behavior ranging from spontaneous regression to highly aggressive disease resistant to all currently available treatment modalities.[1] New treatment approaches, in particular, in advanced disease, are therefore urgently required.

In neuroblastoma, high numbers of microvessel counts have been described,[2,3] as well as frequent angiogenic growth factor expression such as vascular endothelial factor (VEGF). Furthermore, downregulation of the physiological angiogenic growth inhibitors actinin A and thrombospondin correlate with advanced stages.[4–6] Tumor angiogenesis may therefore

Key words: VEGFR1-3 tyrosine kinase inhibitor, axitinib, rapamycin, microvessel density, circulating endothelial cells, childhood neuroblastoma

Abbreviations: CEC: circulating endothelial cells; CEP: circulating endothelial progenitor cells; CMC: carboxyl methylcellulose; DMEM: Dulbecco's modified Eagle's medium; DMSO: dimethyl sulfoxide; EDTA: ethylenediaminotetraacetic acid; FCS: fetal calf serum; HES: hematoxylin–eosin–safranin; IC_{50}: half maximal inhibitory concentration; IHC: immunohistochemistry; mTOR: mammalian target of rapamycin; MTS: (3-(4,5-dimethylthiazol-2-yl)-5-(3-carboxymethoxyphenyl)-2-(4-sulfophenyl)-2H-tetrazolium); MVD: microvessel density; OSFD: overall surface fraction of tumor vessels; PBS: phosphate buffer saline; PI3-K: phosphatidyl inositol 3 kinase; PVDF: polyvinylidene difluoride; SDS: sodium dodecyl sulfate; TGD: tumor growth delay; VEGF: vascular endothelial growth factor; VEGFR: vascular endothelial growth factor receptor

This work was presented, in part, at the 21st AACR-NCI-EORTC International Conference on Molecular Targets and Cancer Therapeutics in Boston, MA, in 2009 (Proceedings, p166, B1, #695)

Grant sponsors: European Union (6th Framework Progamme KidsCancerKinome), DAAD-INCa Joint Transnational Research Programme on Cancer

DOI: 10.1002/ijc.25611

History: Received 11 Mar 2010; Accepted 21 Jul 2010; Online 16 Aug 2010

Correspondence to: Birgit Geoerger, Institut Gustave Roussy, UPRES EA 3535, Pharmacology and New Anticancer Treatments, 39 Rue Camille Desmoulins, 94805 Villejuif, France, Tel.: +33-1-42-11-46-61, Fax: +33-1-42-11-52-45, E-mail: geoerger@igr.fr

represent a promising therapeutic target, especially when metastases are present.[7] While antiangiogenic compounds have defined a role in the management of adult cancers,[8] its utility in the management of pediatric malignancies has not been explored to the same extent.

Tumor angiogenesis is a complex process involving multiple pro- and antiangiogenic factors. Consequently, inhibiting this process using single or multiple agents, with or without inhibitors of downstream effectors, remains a field of intensive research. The VEGF/VEGF receptor (VEGFR) signaling pathway through activation of PI-3K/AKT/mTOR downstream effectors plays a pivotal role in tumor angiogenesis. Several agents, such as the monoclonal anti-VEGF antibody bevacizumab, the multikinase inhibitors sunitinib (targeting VEGFR-2, PDGFR, KIT and Flt-3) and sorafinib (anti-VEGFR-2, PDGFR, b-Raf, Flt-3 and KIT) targeting this pathway have been received approval for the treatment of cancers. Preclinical studies reported antitumor effects of bevacizumab, sunitinib and vandetanib in neuroblastoma.[9–13] In addition to the inhibition of the sprouting process originating from blood vessels in the surrounding of new tumors, the recently described participation of circulating endothelial cells (CECs) in tumor angiogenesis, the circulating endothelial progenitors from the bone marrow (CEPs), as well as mature CECs seem to represent additional targets for antiangiogenic strategies.[14] In neuroblastoma, statistically higher numbers of CEPs have been detected in patients with metastasized pediatric solid tumors, including stage 4 neuroblastoma.[15]

Axitinib (AG-013736) is a novel, potent, small molecule tyrosine kinase inhibitor that selectively inhibits VEGFR-1, -2 and -3 at sub-nanomolar concentrations. Axitinib inhibits angiogenesis, vascular permeability and blood flow.[16] In nonclinical models, axitinib inhibited the growth of primary tumors in human xenografts by interacting with tumor angiogenesis in colorectal, breast, melanoma and glial tumors. It also decreased metastasis to lung and lymph nodes in murine lung and melanoma models.[17] Axitinib has shown promising single agent activity in advanced malignancies.[18–21] It was granted orphan drug status by the US Food and Drug Administration (FDA) in 2007 for the treatment of pancreatic cancer.[22] Accrual to two Phase III randomized clinical trials of axitinib in the treatment of renal and pancreatic cancers, as a single agent and in combination therapy, respectively, has been completed.

Our study explored the preclinical activity of axitinib in human neuroblastoma, its combination with the mTOR antagonist rapamycin, as well as the angiogenesis mechanisms involved.

Material and Methods

Drugs

Axitinib (AG-013736) was provided by Pfizer (La Jolla, CA) as a white to light yellow crystalline powder and stored, protected from light, at 4°C. For *in vitro* use, a 10 nmol/l stock solution in dimethylsulfoxide (DMSO) was stored at −20°C. For *in vivo* experiments, axitinib was formulated once every 7–10 days in a homogeneous suspension of 0.5% carboxyl methylcellulose (CMC; ICN Pharmaceuticals SA, Orsay, France) while protected from light and at 4°C during the studies. Rapamycin was purchased from LC Laboratories (Woburn, MA), stored at −20°C, and diluted in ethanol for stock solution and water for final use.

Cell lines and xenografts

The IGR-N91 cell line and xenograft were derived from the bone marrow of chemotherapy-pretreated stage 4 neuroblastoma of an 8-year-old boy.[23] The IGR-NB8 cell line was derived from a primary stage 3 abdominal neuroblastoma of a 5-year-old boy.[24] The cell lines LAN-5, IMR-32, SK-N-SH, SK-N-BE and SH-SY5Y were kindly provided by Dr. A. Valent (Genetic unit, Institut Gustave Roussy). All neuroblastoma cell lines were cultured in Dulbecco's modified Eagle's medium (DMEM) containing 10% fetal calf serum (all Invitrogen SARL, Cergy Pontoise, France). HUVEC cells (purchased from Cell Applications, p/a Tebu-Bio, Le Perray en Yvelines, France) were grown in endothelial cell basal medium-2 (EMB®-2, Lonza, Basel, Switzerland) supplemented the recommended growth factor mixture (BBE, FBS, hEGF, GA1000 and hydrocortisone) and with 10% fetal calf serum.

MTS cell proliferation assay

HUVEC, SH-SY5Y, IGR-N91 and IGR-NB8 cell lines were seeded at 5,000 cells per well in a 96-well plate and left to settle overnight in EMB®-2 or DMEM with 10% fetal calf serum. The cells were treated with axitinib at concentrations ranging from 1 nmol/l to 10 μmol/l. Cell viability was determined after 72 hr using MTS tetrazolium substrate (CellTiter 96 Aqueous One Solution Cell Proliferation Assay; Promega Corporation, Charbonnieres, France) and colorimetric measurement at 490 nm in an automatic plate reader (Elx808; Fisher Bioblock Scientific SAS, Illkirch, France). IC_{50} values were calculated using GraphPad® Prism software (version 3.00).

Experimental in vivo studies

All animal experiments were carried out under the conditions established by the European Community (Directive 86/609/CCE). IGR-N91 tumor fragments (30 mm^3) were xenotransplanted subcutaneously in the right flank of female SPF-Swiss athymic nude mice at 6–8 weeks of age. After 3–4 weeks, animals bearing subcutaneous tumors of 100–300 mm^3 were randomly assigned to treatment groups on Day 0 (*i.e.*, the start of treatment). Axitinib was administered at 30 mg/kg BID per oral gavage for 2 weeks; control animals received 0.5% CMC. Rapamycin was administered intravenously at 20 mg/kg every 2 days for five administrations (q2d×5). Tumors were measured twice weekly and volumes calculated according to the equation: V (mm^3) = width^2 (mm^2) × length (mm)/2. The experiments continued until tumor volumes reached 1,500 mm^3. Tumor doubling time (T_d) was determined in the exponential growth phase between 200 and 400 mm^3 by

using cubic spline fitted curves and graphs in the Prism program. Therapeutic activity was evaluated by complete and partial tumor regression (*i.e.*, total tumor regression or tumor volume <15 mm^3 and $>50\%$ decrease in tumor volume, respectively, in at least two consecutive measurements), tumor growth delay (TGD; median time in days to reach five times initial tumor volume of treatment group compared to controls) and number of tumor-free survivors at Day 120.

For the orthotopic neuroblastoma model, 1×10^6 IGR-N91 cells, transfected with a pcDNA3 plasmid wearing *LUC* gene to express firefly luciferase, were injected into the left adrenal in NOD/Scid mice under general anesthesia procedure with isoflouran. Axitinib 30 mg/kg BID was administered for 19 days starting at Day 4 after transplantation (with a 2-day holiday after 12 days). Tumor growth was followed by bioluminescence imaging using IVIS® 50 (Caliper Life Science S.A., Trembley, France) once or twice weekly. Mice were sacrificed at Day 18 and tumor load was estimated by bioluminescence imaging.

The two-tailed nonparametric Mann–Whitney or Kruskal–Wallis test and Prism software was used to determine statistical significance of the median time to reach five times initial tumor volume or bioluminescence uptake.

Western immunoblotting

Cell or tumor lysates were isolated using lysis buffer containing 50 nM Tris HCl (pH 8.0), 0.5% IGEPAL, 0.3% Triton X100, 5 mM $MgCl_2$, 0.5 mM EDTA, 1 mM DTT, 10% glycerol, protease and phosphatase inhibitor cocktail tablets (Complete mini, Roche Diagnostics, Meylan, France). Equal amounts of protein (40 μg) were separated by 7% SDS-PAGE and electrophoretically transferred on to hydrophobic polyvinylidene difluoride (PVDF) membranes optimized for protein transfer (Hybond-P; Amersham Biosciences, Orsay, France). The membranes were probed after a blocking procedure with the mouse monoclonal antibodies anti-human VEGFR-1 (Flt-1; 1:1,000), human VEGFR-2/KDR (1:1,000; both R&D Systems Europe, Lille, France), human VEGFR-3 (1:1 000; RELIA*Tech*GmbH, Wolfenbuettel, Germany), the rabbit monoclonal antibody phospho-VEGFR-2 (Tyr1175; 19A10), the rabbit polyclonal anti-human AKT, phospho-AKT (Ser473), MAPK, phospho-MAPK (Thr202/Tyr204), all diluted to 1:1,000 (all Cell Signaling Technology®, Ozyme, St Quentin-en-Yvelines, France), and revealed using horseradish peroxidase goat conjugated anti-mouse or anti-rabbit IgG antibody, respectively, diluted to 1:5,000 (Amersham Biosciences) and enhanced chemiluminescent substrate (SuperSignal West Pico, Thermo Scientific, p/a Perbio Science France SAS, Brebières, France).

Immunohistochemistry and determination of microvessel density and surface fraction

IGR-N91 tumors in nude mice treated with axitinib or CMC during 2 weeks were harvested and fixed in FineFix® (Milestone, Bergamo, Italy) and paraffin-embedded. Four-micrometer sections were incubated following heat-induced antigen retrieval and blocking serum (Power Block 1:10; BioGenex, Marseille, France) with purified rat anti-mouse CD34 antibody (1:20; Hycult Biotechnology, The Netherlands) and rabbit anti-rat secondary antibody (1:400; Southern Biotech, Montrouge, France). Immunostaining was visualized using the peroxidase/diaminobenzidine chromogenic substrate Rabbit PowerVision Kit (ImmunoVision Technologies, Brisbane, CA).

Images of the whole histological sections were recorded using a Nikon SuperCoolscan 8000 ED slide scanner equipped with a FH-8G1 medical slide holder (Nikon, Champigny-sur-Marne, France), prenecrotic and necrotic surface areas excluded, and analyzed by an automatic procedure using PixCyt® image analysis software (GRECAN (Groupe Regional d'Etudes sur le Cancer), Centre François Baclesse, Caen, France.[25] The resolution was 4,000 dots per inch with 1 pixel covering an area of 40 μm^2. The microvessel density (MVD) profiles are expressed as the number of vessels per square millimeter and as surface fraction (%) of tumor tissue.

Measurement of CECs and CEPs

Whole blood (~250 μl) was drawn through retro-orbital venous puncture on Days 0, 7, 14, 21 and 28 from mice bearing IGR-N91 xenografts during axitinib treatment at 30 mg/kg BID for 2 weeks. CEC and CEP counts were measured by four-color flow cytometry as previously reported (unpublished data, Taylor *et al.*, submitted). Briefly, CECs were detected using the rat anti-mouse monoclonal antibodies anti-MECA-32 biotin, anti-CD31 FITC, anti-CD45 PerCP, anti-Flt-1 PE and streptavidin-APC (all BD Pharmingen, NJ). CEPs were detected using the rat anti-mouse monoclonal antibodies anti-Sca-1-FITC or anti-CD31-FITC, anti-Flk-1-PE, anti-CD45-PerCP and anti-CD-117-APC (all BD Pharmingen). Isotypic control tubes included fluorochrome-conjugated rat anti-mouse isotypic controls. Cells were acquired on a FACSCalibur and analyzed by CELLQuest 3.2 software (both BD Biosciences). Additionally, white blood cell counts were determined for each murine blood sample using a MS9-3 counter (Melet Schloesing, Osny, France) for calculations of absolute counts of CECs and CEPs.

The variation of the CEP and CEC numbers in blood through the time from Day 0 to Day 28 was assessed by examining the time-concentration relationship. The primary parameter was the population-averaged slope α determined by using the linear mixed model:

$$y_{ij} = \beta_0 + (\alpha + a_i)^* t_{ij} + e_{ij}$$

where y_{ij} is the response (CEP or CEC blood concentration) of the mouse i at the day j, $\beta_0 + (\alpha + a_i)^* t_{ij}$ is the expected value of the response for the mouse i at the day t_{ij}, which illustrate a linear relation between the response and the time with a slope $(\alpha + a_i)$ and an intercept β_0, β_0 is the baseline mean response, t_{ij} is the day j of measurement of the response on the mouse i, considered as a continuous

quantitative covariate (0 for the Day 0, 1 for the Day 1, 2 for the Day 2, etc.), $(\alpha + a_i)$ is the subject-specific slope of the mouse i, α is the mean if these slope in the population (called population-averaged slope in the mixed model literature) and a_i is an individual random effect and e_{ij} is the random error term for mouse i at the day j.

All data from a given mouse were included in this model; statistical analysis was performed using the mixed procedure of the SAS software which determined the p value of the test of the null hypothesis $\alpha = 0$, which is equivalent to the fact that the blood concentration of the CEC or CEP do not vary with time in the population.

A mixed E_{max} model[26,27] was fitted for the CEP data using the Nlmixed procedure of the SAS software. This model fits better these data than the linear mixed model, but it was not possible to fit it for the CEC data. This model is explained by the following equation:

$$\mathrm{CEP}_{ij} = E_0 + \frac{(E_{\max} + a_{1i})^* t_{ij}}{(\mathrm{ED}_{50} + a_{2i}) + t_{ij}} + e_{ij}$$

where CEP_{ij} is the CEP blood concentration of the mouse i at the day j, $E_0 + \frac{(E_{\max}+a_{1i})^* t_{ij}}{(\mathrm{ED}_{50}+a_{2i})+t_{ij}}$ is the expected value of the CEP response for the mouse i at the day t_{ij}, E_0 is the basal effect, corresponding to the mean response when the time is zero (before administration of the drug), $E_{max} + a_{1i}$ is the maximum effect attributable to the drug for the mouse i, E_{max} is the mean of these maximum effects through the population of all mice (or its typical value in this population) and a_{1i} is a random individual effect. $\mathrm{ED}_{50} + a_{2i}$ is the time in which half of E_{max} is produced for the mouse i, ED_{50} is the mean of these times in the population of all mice (or its typical value in this population) and a_{2i} is a random individual effect.

The expected value of the E_{max} model $(E_0 + \frac{(E_{\max}+a_{1i})^* t_{ij}}{(\mathrm{ED}_{50}+a_{2i})+t_{ij}})$ illustrates the fact that the expected value of the response can increase or decrease hyperbolically. If the response is decreasing, the value of the E_{max} parameter will be negative. Note the difference between E_{max}, which is the maximal effect attributable to the drug, and $(E_0 + E_{max})$, which is the asymptotic response. The E_{max} model is usually used to model the monotonous not linearity with an effect threshold $(E_0 + E_{max})$.

Our parameter of interest in this study is the E_{max} parameter, which characterizes the population; the fact that it is equal to zero is equivalent to the fact that the mean of the response is constant in this population. The p value of the test of the null hypothesis $E_{max} = 0$ was obtained.

Results

VEGFR-2 and VEGFR-3 are expressed on neuroblastoma cells

All neuroblastoma cell lines tested, LAN-5, IMR32, SK-N-SH, SK-N-BE, SH-SY5Y, IGR-NB8 and IGR-N91, exhibited VEGFR-2 expression as shown by Western blot analysis (Fig. 1).

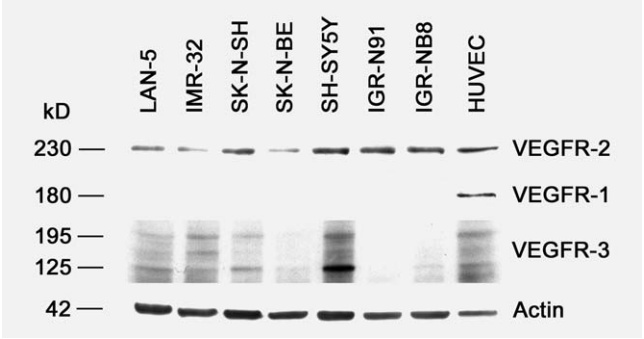

Figure 1. Expression of VEGFR-1, VEGFR-2 and VEGFR-3 in neuroblastoma cell lines. Protein lysates of the LAN-5, IMR32, SK-N-SH, SK-N-BE, SH-SY5Y, IGR-NB8 and IGR-N91 neuroblastoma cell lines were resolved by electrophoresis on 7% SDS-PAGE, transferred to PVDF membrane and visualized using Western blotting with specific antibodies to VEGFR-1, VEGFR-2 and VEGFR-3 (1:1,000), detected with anti-mouse antibodies (1:5,000) and enhanced chemiluminescent substrate. The blots were reprobed with anti-actin as loading control. HUVEC cells were used as controls.

We further found VEGFR-3 expressed in LAN-5, IMR-32, SK-N-AS and SH-SY5Y, but not in SK-N-BE, IGR-NB8 and IGR-N91. VEGFR-1 expression was not found on the cell lines tested compared to the positive HUVEC cells.

Axitinib reduces neuroblastoma cell proliferation in vitro

HUVEC and the IGR-N91, IGR-NB8 and SH-SY5Y neuroblastoma cell lines were cultured under standard conditions and treated with axitinib at concentrations ranging from 1 nmol/l to 10 μmol/l. Axitinib reduced cell viability in a dose-dependent manner with IC_{50} doses of >10,000, 849 and 274 nmol/l for IGR-N91, IGR-NB8 and SH-SY5Y, respectively, as measured by MTS assay at 72 hr (Fig. 2). In our hands, the sensitivity to axitinib of neuroblastoma cell lines appeared to be in a similar range as non-VEGF stimulated HUVEC (IC_{50}, 573 nmol/l), whereas IC_{50}s 1,000 times lower had been reported in the literature for VEGF-stimulated endothelial cells HUVEC (IC_{50}, 0.17 nmol/l).[17]

Axitinib exhibits significant antitumor activity against neuroblastoma flank xenografts alone and in combination with rapamycin

Axitinib was first evaluated as a single agent *in vivo* against IGR-N91 flank xenografts at advanced tumor stage (Table 1, AG-013736 (axitinib) alone and Fig. 3*a*). Athymic mice bearing tumors of 50–262 mm^3 were randomly assigned 25 days after transplantation to treatment groups of 11 tumors each. According to prior experiments in various human cancer models showing maximum growth inhibiting effects,[17] axitinib was administered orally at a dosage of 30 mg/kg BID for 14 days; control animals received 0.5% carboxyl methylcellulose in equivalent amount and schedule. Control tumors grew

with a median tumor doubling time of 4.8 days (range, 3.5–8.7 days) and reached a median of five times initial tumor volume at 14 days (range, 9.3–17.6 days). Axitinib treatment did not result in partial or complete tumor regression and the median time to reach five times initial tumor volume was 25.4 days (range, 15.7–34.6 days), representing a significant difference in tumor growth delay of 11.4 days when compared to the controls ($p = 0.0006$; Mann–Whitney test).

VEGFR signaling activates downstream effectors such as AKT and mTOR suggesting that combinations with one of their inhibitors may have superior activity. We therefore further explored the activity of the mTOR inhibitor rapamycin in combination with axitinib against IGR-N91 xenografts (Table 1, AG-013736 (axitinib) and rapamycin and Fig. 3*b*). As observed in the first experiment, axitinib resulted in significant tumor growth delay of 17.7 days compared to controls ($p < 0.01$; Kruskal–Wallis test); the median time to reach five times initial tumor volume was 27.2 days (range, 19.3–29.6 days) compared to 9.5 days (range, 7.9–26.2 days) in controls which exhibited a median tumor doubling time of 3.9 days (2.4–4.8 days). Tumors treated with rapamycin administered intravenously at 20 mg/kg every 2 days for five doses reached a median of five times initial tumor volume at 20.5 days (range, 18.9–27.8 days), thus a median tumor growth delay of 11.5 days compared to controls (ns). Simultaneous administration of both agents resulted in a median five times initial tumor volumes of 26.0 days (range, 21.4–30.1 days) and thus a significant median tumor growth delay of 16.5 days ($p < 0.01$), which was however not enhanced compared to axitinib alone.

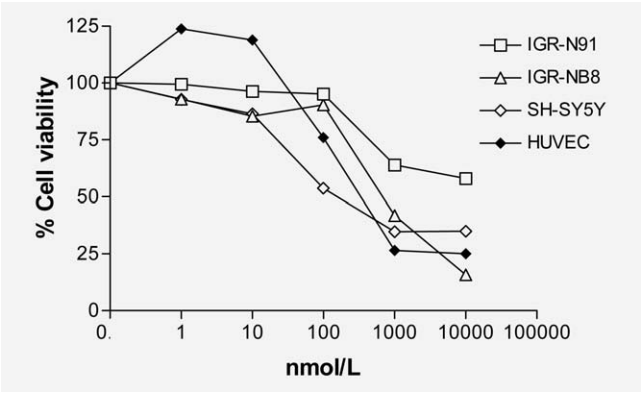

Figure 2. Antiproliferative activity of axitinib in neuroblastoma cell lines. Neuroblastoma cell lines IGR-N91, IGR-NB8, SH-SY5Y and HUVEC cells were cultured in DMEM supplemented with 10% fetal calf serum or EMB®-2 and treated with axitinib at concentrations ranging from 1 nmol/l to 10 μmol/l. Cell viability was measured by MTS proliferation assay at 72 hr.

Axitinib exhibits significant antitumor activity against orthotopic neuroblastoma xenografts

To explore antitumor effects in a relevant *in vivo* model, we used a recently developed orthotopic model of IGR-N91 injected into the left adrenal of NOD/Scid mice. Treatment with axitinib 30 mg/kg or equivalent 0.5% CMC BID was started at Day 4 after transplantation. All animals developed local tumors as measured by bioluminescence imaging. Treatment of axitinib for 18 days resulted in reduced bioluminescent signals as compared to controls ($p = 0.0262$ in Mann–Whitney test; Fig. 3*c*).

Axitinib inhibits VEGFR-2 phosphorylation in neuroblastoma xenografts in vivo

We next explored the mechanism of axitinib treatment *in vivo* in the IGR-N91 flank model. Animals bearing IGR-N91 tumors were treated with axitinib at 30 mg/kg BID or methylcellulose during 14 days; then tumors were harvested and protein lysates were subjected to Western blot analysis. Treatment with axitinib resulted in downregulation of VEGFR-2 phosphorylation in all three IGR-N91 xenograft tumor samples compared to controls. However, downstream effectors such as activated AKT and MAPK were not inhibited (Fig. 4*a*).

Table 1. Antitumor activity of AG-013736 alone and with rapamycin against IGR-N91 xenografts

	Treatment schedule	Tumor (*n*)	Tumor volume, Mean (range) (mm^3)	DT	5 × V_i (days)	TGD (days)	*p*
AG-013736 (axitinib) alone							
CMC 0.5%	0.2 ml BID × 2w	11	122 (50–230)	4.8	14.0		
AG-013736	30 mg/kg BID × 2w	11	136 (62–262)		25.4	11.4	0.0006
AG-013736 (axitinib) and rapamycin							
CMC 0.5%	0.2 ml BID × 2w	8	71 (53–101)	3.9	9.5		
AG-013736	30 mg/kg BID × 2w	8	78 (55–110)		27.2	17.7	<0.01
Rapamycin	20 mg/kg q2d × 5	6	128 (103–155)		20.9	11.5	ns
AG-013736&	30 mg/kg BID × 2w	6	69 (64–73)		26.0	16.5	<0.01
Rapamycin	20 mg/kg q2d × 5						

DT: tumor doubling time; median 5× V_i: five times initial tumor volume; TGD: tumor growth delay; *p* for statistical difference, median 5× initial tumor volumes in treatment groups were compared using a two-tailed nonparametric Mann–Whitney or Kruskal–Wallis test for two or multiple groups, respectively.

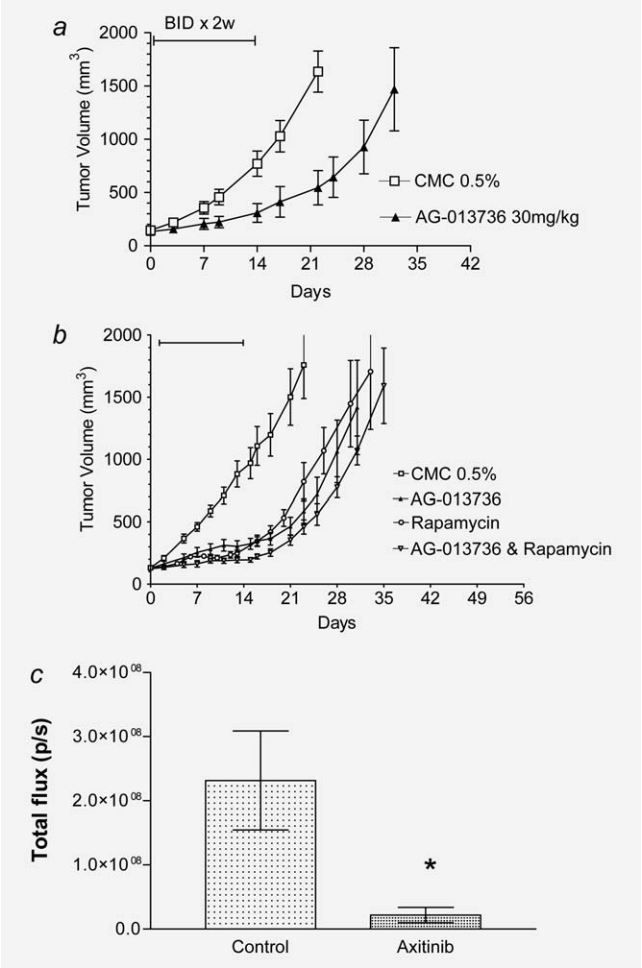

Figure 3. Antitumor activity of axitinib alone and in combination with rapamycin against IGR-N91 xenografts. (*a*) Animals bearing IGR-N91 flank xenograft tumors received at advanced tumor stage axitinib orally per gavage 30 mg/kg BID for 2 weeks or 0.5% carboxyl methylcellulose (CMC) in equivalent schedule for controls. Data are representative of the mean ± standard error of the mean (SEM) for each treatment group. (*b*) Animals bearing IGR-N91 flank xenograft tumors were treated by 0.5% CMC, oral axitinib at 30 mg/kg BID for 14 days, rapamycin at 20 mg/kg intravenously every 2 days × 5, or both agents simultaneously. Data are representative of the mean ± SEM for each treatment group. (*c*) NOD/Scid mice were injected with 1×10^6 IGR-N91-Luc cells into the left adrenal on Day 0 and treated with 0.5% CMC or axitinib 30 mg/kg BID starting from Day 4 during 18 days. Bioluminescence was estimated using the IVIS 50® once or twice weekly. Graph shows mean bioluminescence ± SEM as measured *in vivo* on Day 18 in vehicle- and axitinib-treated animals; *statistical significance in bioluminescence between axitinib and controls as determined by Mann–Whitney test.

Axitinib reduces MVD and overall surface fraction of tumor vessels in neuroblastoma xenografts

IGR-N91 flank tumors treated with axitinib or methylcellulose during 14 days were harvested at Day 14 and analyzed for CD34 staining by immunohistochemistry. Axitinib treatment resulted in significant reduction of tumor vascularization as shown by CD34 immunohistochemical staining (Fig. 4*b*). The MVD per square meter determined was 21.27 ± 10.03 in treated tumors compared to 48.79 ± 17.27 in controls ($p = 0.0023$; Mann–Whitney test) (Fig. 4*c*). This antitumor vessel activity was confirmed by determining the overall surface fraction of tumor vessels (OSFV), which was 0.56% ± 0.17% in treated tumors versus 1.29% ± 0.37 in controls ($p = 0.0006$; Fig. 4*d*).

Axitinib therapy decreases the numbers of CEP but not CEC in mice bearing neuroblastoma xenografts

CECs and CEPs are currently being investigated in a variety of diseases as markers of vascular turnover or damage and, also in the case of CEPs, vasculogenesis, as well as their role as potential surrogate markers for monitoring antiangiogenic therapy. Therefore, we measured CEC and CEP levels by four-color flow cytometric assay in whole blood in athymic mice bearing advanced IGR-N91 tumors drawn before, on Days 7 and 14 during axitinib treatment as well as on Day 21 and 28, *i.e.*, during 14 days after stop of treatment. Mean (±SD) CEC numbers were 0.27 ± 0.08, 0.31 ± 0.11, 0.08 ± 0.18, 0.10 ± 0.10 and 0.38 ± 0.45 cells/μl at baseline, on Days 7, 14, 21 and 28, respectively. CEPs were reduced during the axitinib treatment and for at least 14 days after the end of treatment: 0.40 ± 0.08, 0.02 ± 0.03, 0.00 ± 0.01, 0.08 ± 0.10 and 0.03 ± 0.02 cells/μl before treatment and on Days 7, 14, 21 and 28, respectively. We wished to develop a model that allows statistical evaluation of these potential biomarkers and their variation with time of treatment. When applying a mixed linear model on all data, no significant modification was confirmed for numbers of CECs ($p = 0.4556$; Fig. 5*a*). For CEPs, both a mixed linear and mixed E_{max} model (Fig. 5*b*) were applied and showed a significant decrease in the CEP levels over time ($p = 0.0096$ and 0.0007, respectively). The Akaike information criteria (AIC: −19.6 *vs.* −42.8, respectively), bias-corrected Akaike information criteria corrected (AICC: −19.5 *vs.* −39.3) and the Bayesian information criteria (BIC: −19.5 *vs.* −42.2) values showed that the E_{max} model was more adequate for these data than the linear model. The graphs suggested further that the CEP observation on Day 21 for mouse 35 could be a potential outlier; an exclusion of this observation resulted in a p value of 0.0002 for the E_{max} parameter of the mixed E_{max} model. Thus, CEP could represent a pharmacodynamic marker for antiangiogenic treatment.

Discussion

Axitinib has been developed as a selective inhibitor of VEGFR-1, −2 and −3. In comparison to the multikinase inhibitors sunitinib and sorafenib that also have an inhibitory activity on several other tyrosine kinase receptors, which are also expressed on tumor cells,[28] it has demonstrated an antiangiogenic activity that is stronger and more specific. We

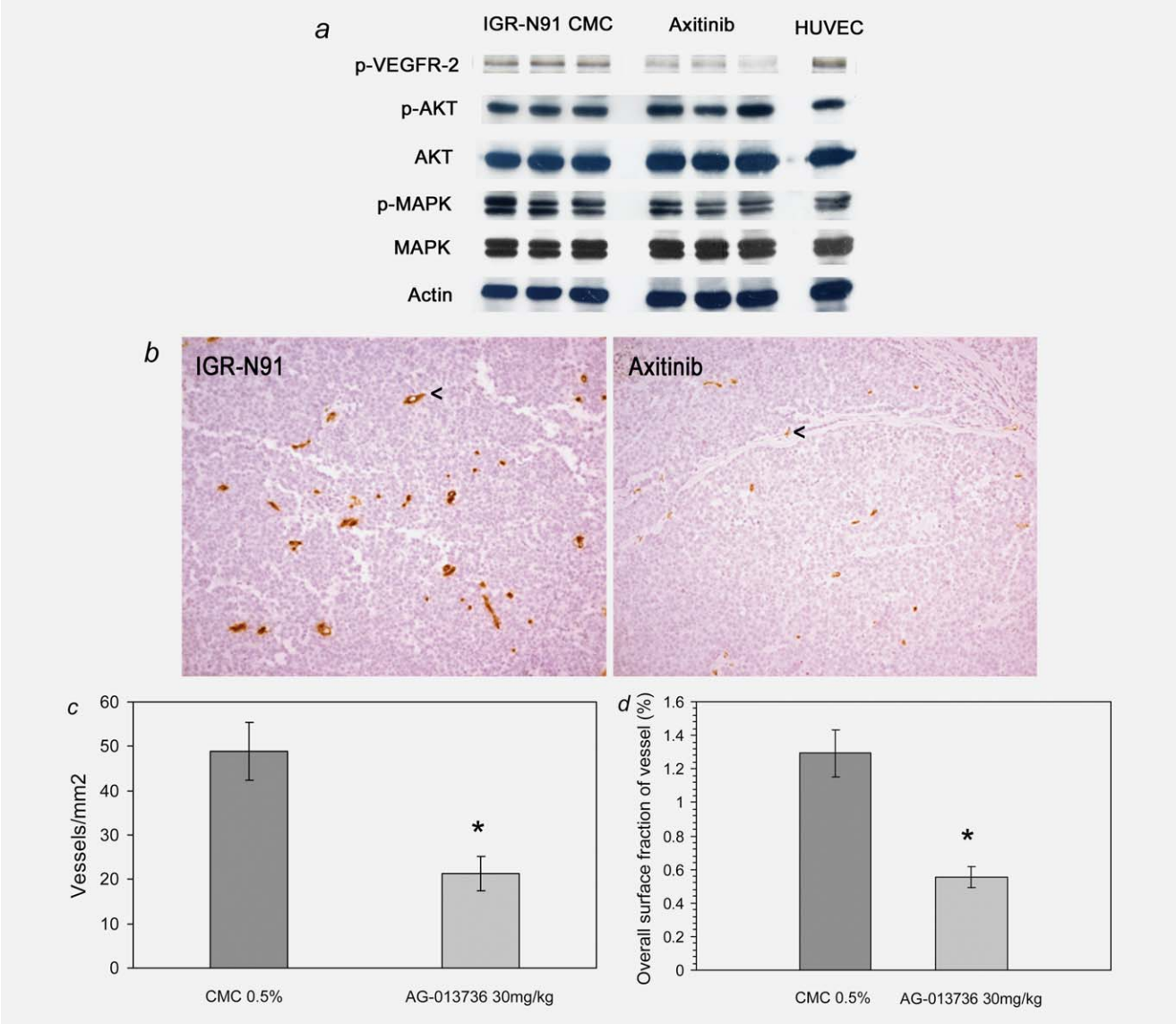

Figure 4. Axitinib inhibits VEGFR-2 phosphorylation resulting in reduced microvessel density. IGR-N91 xenograft tumors were harvested after treatment with axitinib 30 mg/kg or CMC 0.5% BID for 14 days and subjected to Western blotting or immunohistochemistry. (*a*) Protein lysates of IGR-N91 tumors were resolved by electrophoresis on 7% SDS-PAGE, transferred to PVDF membrane and visualized using Western blotting with specific antibodies to p-VEGFR-2, AKT, p-AKT, MAPK and p-MAPK, detected with anti-mouse antibodies (1:5,000) and enhanced chemiluminescent substrate. The blots were reprobed with antiactin antibody as loading control. (*b*) Immunohistochemical staining of the endothelial cell marker CD34 shows reduced microvessel density in tumors treated with axitinib (right panel) compared to CMC (left panel). Figures show representative tumors at an original magnification of ×100; vessels are highlighted by arrows. The microvessel density profiles are expressed as the number of vessels per mm^2 (*c*) and as surface fraction (%) of tumor tissue (*d*) using PixCyt® image analysis software. *statistical significance in numbers of vessels and surface fraction between axitinib and controls as determined by Mann–Whitney test. [Color figure can be viewed in the online issue, which is available at wileyonlinelibrary.com.]

have shown antiproliferative effects of axitinib on neuroblastoma cell lines and significant antitumor activity against neuroblastoma flank and orthotopic models *in vivo*. Axitinib exhibited a dose-dependent inhibition of human neuroblastoma cell lines at IC_{50} from 274 to10,000 nmol/l. This compares favorably to results reported for the VEGFR-2/EGFR tyrosine kinase inhibitor vandetanib with IC_{50} doses between 1 and 10 μmol/l,[12] but unfavorably with those reported for the multitargeted VEGFR-2 inhibitor sunitinib that targets PDGFR, KIT and Flt-3 next to VEGFR-2 with IC_{50} of 10–20 ng/ml (25–50 nmol/l) in neuroblastoma cells.[10] The IC_{50} value of axitinib reported for VEGF-stimulated endothelial cell HUVEC is 1,000 times lower[17]; however, nonstimulated HUVECs showed a IC_{50} of 573 nmol/l in our experimental

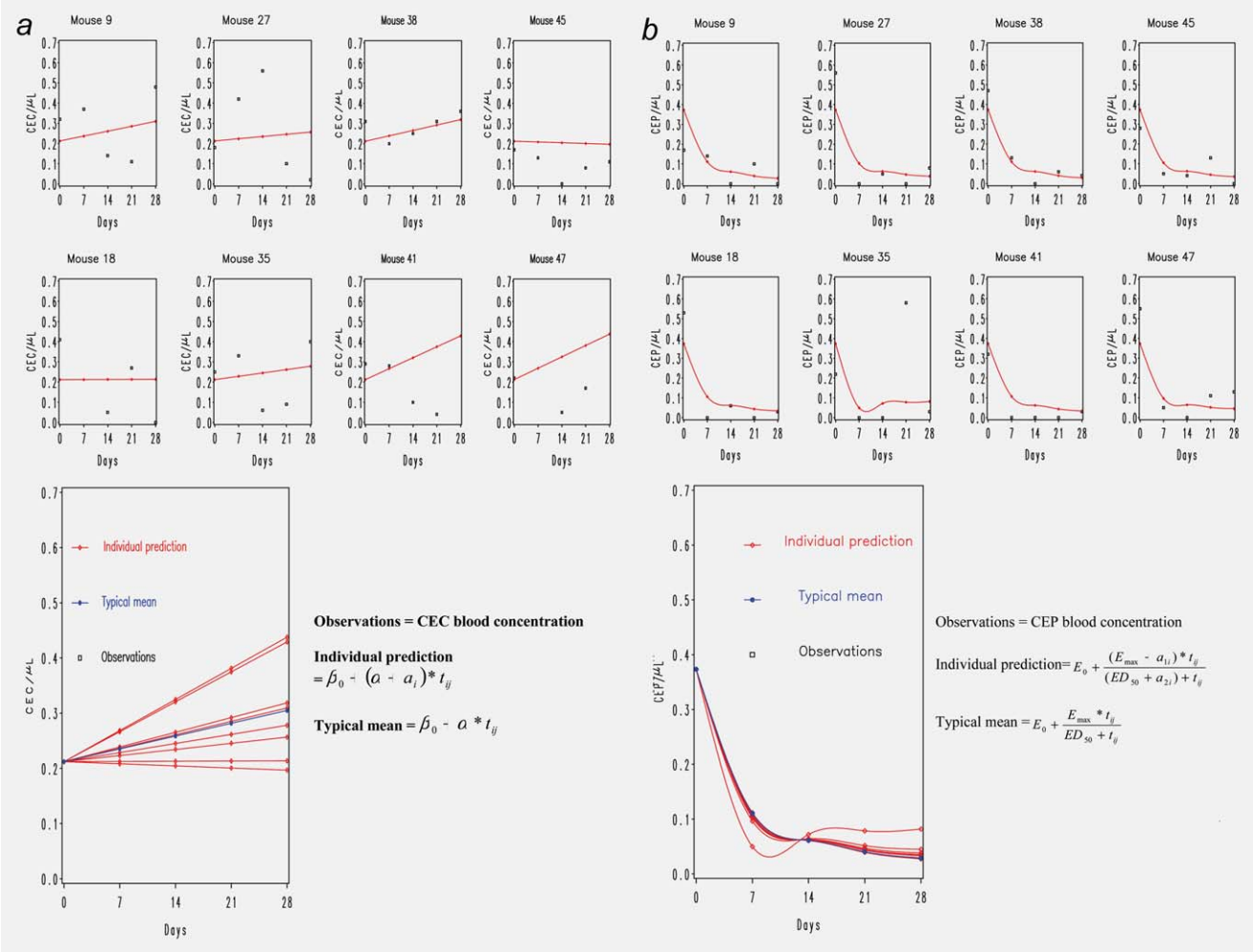

Figure 5. Circulating endothelial progenitor cells (CEPs) and circulating endothelial cells (CEC) during therapy with axitinib. Whole blood was drawn on Days 0, 7, 14, 21 and 28 from mice bearing IGR-N91 xenografts before, during and after axitinib treatment at 30 mg/kg BID for 14 days. CECs and CEPs were determined by four-color flow cytometry using anti-MECA-32, CD31, CD45, Flt-1 (VEGFR-2) and streptavidin, and anti-Sca-1 or CD31, Flk-1, CD45 and CD117, respectively. Graphs show individual numbers of CEC (*a*) and CEP (*b*) in each mouse treated and an applied linear and E_{max} model, respectively. The lower graphs show each individual prediction and the typical mean for all eight mice. Axitinib did not reduce CECs ($p = 0.4556$; linear model), but CEPs during at least 28 days ($p = 0.0007$; E_{max} model). [Color figure can be viewed in the online issue, which is available at wileyonlinelibrary.com.]

setting. The VEGF/VEGFR pathway seems to act primarily by promoting angiogenesis, but it may also function through promoting neuroblastoma cell growth directly.[29] In addition to the expression of VEGFR-2, VEGFR-1 expression may be required for cytotoxic effects on tumor cells. None of the neuroblastoma cell lines tested here expressed VEGFR-1 whereas VEGFR-3 and VEGFR-2 was present in several or all of them. The results of studies of VEGFR expression in neuroblastoma have been conflicting. Most studies of neuroblastoma cell lines could not demonstrate an autocrine effect of VEGF/VEGFR.[4,30,31] Although data on tumor specimens showed VEGFR-2 and VEGFR-1 expression, their origin (tumoral or endothelial) remain unclear.[32] *In vivo* administration of axitinib 30 mg/kg, the dose which has been shown to result in maximum growth inhibiting effects in other xenograft models, resulted in inhibition of VEGFR-2 phosphorylation and led to significant antitumor effects on established IGR-N91 tumors. The antiangiogenic effects of axitinib against neuroblastoma xenograft tumor vasculature, as measured by morphology, MVD and OVSD, were reduced in all treated tumors compared to controls. However, no significant morphological cell death features were observed in neuroblastoma tumor cells. Axitinib resulted in a reduction in neuroblastoma tumor growth compared to controls although no tumor regression was observed in the three independent *in vivo* experiments. This is similar to the prior findings on axitinib, inhibiting tumor growth in a wide range of different adult cancer xenograft models.[17] We have shown that despite

the inhibitory effects of axitinib on constitutive VEGFR-2 phosphorylation, its downstream effector pathways PI-3K/AKT/mTOR and RAS/MAPK are not inhibited in IGR-N91 xenografts. Both cell signaling pathways are also activated by the majority of growth factor receptors. Several publications have reported that c-kit, PDFGR, EGFR or IGF-1R may play a role in neuroblastoma cell growth. In this regard, we have recently shown that stimulated AKT and MAPK pathways in neuroblastoma cell lines could be reduced by IGF-1R inhibition.[33] The constitutive activation of these downstream effectors tyrosine kinases in IGR-N91 may be a result of activation of other growth factors rather than VEGF/VEGFR and thus their inhibition is not to be expected following unique VEGFR inhibition. Most antiangiogenic compounds are currently being developed in combination with either chemotherapy or other targeted agents. We evaluated the effect of axitinib in combination with the mTOR inhibitor rapamycin. This molecule has been shown to reduce VEGF levels as well as inhibiting endothelial cell proliferation.[34] In our study, rapamycin resulted in tumor growth delay of IGR-N91 xenografts, however, when administered in combination with axitinib, did not result in a significant improvement of its single agent activity. This finding is contrary to recent reports in relation to the multikinase inhibitor sunitinib where low dose sunitinib demonstrated synergistic cytotoxicity with rapamycin.[10] Axitinib in combination with other therapies, such as ionizing radiation,[35] low dose, metronomic cyclophosphamide[28] and docetaxel[17] have shown more promise. Despite the inability to demonstrate tumor regressions in xenograft models, early clinical trials reported objective tumor responses in 30–44% of patients with advanced thyroid or renal cancers,[18,19,36] which needs to be considered for the further development of this angiogenic treatment in children with neuroblastoma.

We recently reported that there is an elevation of CEPs which is related to advanced and metastatic disease in children including those with neuroblastoma.[15] These CEPs, which originate from the bone marrow, showed an important role in the metastatic process and for neuroblastoma to relapse despite the presence of minimal residual disease.[14] We have recently developed a method to determine CECs and CEPs in murine models and have shown that there is an acute and immediate increase of CEPs following treatment with vascular disrupting agents as well as a second burst after 4 days (unpublished data: Taylor *et al.*, submitted). For the phenotypic identification of CEPs, we have chosen to use both progenitor (CD117/Sca-1) and endothelial (VEGFR-2) markers. Pro-angiogenic CEP mobilization has also been reported for certain chemotherapeutic agents.[37] To our knowledge, this is the first time it has been demonstrated that these VEGFR-2 expressing bone marrow derived CEPs were significantly reduced following angiogenic treatment with axitinib. CEPs remained significantly reduced during and at least 14 days after the end of treatment. This finding suggests a role for the use of antiangiogenic agents, such as axitinib, not only for their direct antiangiogenic potential but also for its capacity to reduce chemotherapy-induced rebound effect on these pro-angiogenic cells. Whether CEPs could be useful as pharmacodynamic markers of efficacy for antiangiogenic treatments will need to be determined. In our experience, a mixed E_{max} model was found to be most suitable for these observations; however, this will need to be further explored in higher numbers, possibly within a clinical setting.

Antiangiogenic therapy has emerged as a promising addition to the management of solid tumors. Several antiangiogenic agents have received licensed indications for the treatment of adult tumors in the United States and Europe. Pediatric solid tumors have also been shown to be angiogenesis dependent, especially those tumors at advanced stages.[38] Neuroblastoma is one of the most studied childhood diseases with respect to tumor angiogenesis. Advanced tumors are extremely well vascularized and hence the incorporation of antiangiogenic strategies to current treatment paradigms could potentially provide a significant advance to a disease of high unmet medical need.[7] Although several antiangiogenic agents have been evaluated in phase I pediatric clinical trials, till date, later phase clinical studies have not evaluated the addition of antiangiogenic agents as part of the multimodality treatment of high-risk neuroblastoma. This is the case despite agents such as bevacizumab,[39] sunitinib (Dubois *et al.*, proceedings of ASCO 2008) and sorafenib (Widemann *et al.*, proceedings of ASCO 2009) having been shown to be well tolerated and to having an acceptable toxicity profile similar to that observed in adults. Recommended doses for single agent use have been established for pediatric patients and combination therapies have been started in patients presenting with metastatic rhabdomyosarcoma and non-rhabdomyosarcoma soft tissue sarcomas (BO20924/ITCC-011; NCT00643565) as well as in malignant glioma (NCT00381797 and NCT00890786). Given that the current neuroblastoma protocols for high-risk patients are quite intensive coupled with the young age of these patients, careful thought would be required to define optimal study designs.

In conclusion, our data show that axitinib, a selective antiangiogenic agent, may be a candidate to be explored in the clinical trials involving patients with neuroblastoma. In addition to its well established inhibitory effects on vessel sprouting, we have shown that axitinib has activity against CEPs known to participate in tumor neo-angiogenesis. Its potential for synergism with other agents provides an additional attraction and hence appropriate regimens will need to be further explored in the context of clinical trials of neuroblastoma.

Acknowledgements

We are grateful to Dr. Patrick Gonin and his team at the animal facility of IGR, to Olivia Bawa for her excellent technical assistance. We also thank Drs. Cormac Owens and Louis Viviers for critical reading of the manuscript.

References

1. Maris JM, Hogarty MD, Bagatell R, Cohn SL. Neuroblastoma. *Lancet* 2007;369: 2106–20.
2. Meitar D, Crawford SE, Rademaker AW, Cohn SL. Tumor angiogenesis correlates with metastatic disease, N-myc amplification, and poor outcome in human neuroblastoma. *J Clin Oncol* 1996;14: 405–14.
3. Canete A, Navarro S, Bermudez J, Pellin A, Castel V, Llombart-Bosch A. Angiogenesis in neuroblastoma: relationship to survival and other prognostic factors in a cohort of neuroblastoma patients. *J Clin Oncol* 2000; 18:27–34.
4. Rossler J, Breit S, Havers W, Schweigerer L. Vascular endothelial growth factor expression in human neuroblastoma: up-regulation by hypoxia. *Int J Cancer* 1999; 81:113–7.
5. Yang QW, Liu S, Tian Y, Salwen HR, Chlenski A, Weinstein J, Cohn SL. Methylation-associated silencing of the thrombospondin-1 gene in human neuroblastoma. *Cancer Res* 2003;63: 6299–310.
6. Breit S, Rossler J, Fotsis T, Schweigerer L. N-myc down-regulates activin A. *Biochem Biophys Res Commun* 2000;274:405–9.
7. Rossler J, Taylor M, Geoerger B, Farace F, Lagodny J, Peschka-Suss R, Niemeyer CM, Vassal G. Angiogenesis as a target in neuroblastoma. *Eur J Cancer* 2008;44: 1645–56.
8. Hurwitz H, Fehrenbacher L, Novotny W, Cartwright T, Hainsworth J, Heim W, Berlin J, Baron A, Griffing S, Holmgren E, Ferrara N, Fyfe G, et al. Bevacizumab plus irinotecan, fluorouracil, and leucovorin for metastatic colorectal cancer. *N Engl J Med* 2004;350:2335–42.
9. Segerstrom L, Fuchs D, Backman U, Holmquist K, Christofferson R, Azarbayjani F. The anti-VEGF antibody bevacizumab potently reduces the growth rate of high-risk neuroblastoma xenografts. *Pediatr Res* 2006;60:576–81.
10. Zhang L, Smith KM, Chong AL, Stempak D, Yeger H, Marrano P, Thorner PS, Irwin MS, Kaplan DR, Baruchel S. In vivo antitumor and antimetastatic activity of sunitinib in preclinical neuroblastoma mouse model. *Neoplasia* 2009;11:426–35.
11. Dickson PV, Hamner JB, Sims TL, Fraga CH, Ng CY, Rajasekeran S, Hagedorn NL, McCarville MB, Stewart CF, Davidoff AM. Bevacizumab-induced transient remodeling of the vasculature in neuroblastoma xenografts results in improved delivery and efficacy of systemically administered chemotherapy. *Clin Cancer Res* 2007;13: 3942–50.
12. Beaudry P, Nilsson M, Rioth M, Prox D, Poon D, Xu L, Zweidler-Mckay P, Ryan A, Folkman J, Ryeom S, Heymach J. Potent antitumor effects of ZD6474 on neuroblastoma via dual targeting of tumor cells and tumor endothelium. *Mol Cancer Ther* 2008;7:418–24.
13. Kim ES, Serur A, Huang J, Manley CA, McCrudden KW, Frischer JS, Soffer SZ, Ring L, New T, Zabski S, Rudge JS, Holash J, et al. Potent VEGF blockade causes regression of coopted vessels in a model of neuroblastoma. *Proc Natl Acad Sci USA* 2002;99:11399–404.
14. Bertolini F, Shaked Y, Mancuso P, Kerbel RS. The multifaceted circulating endothelial cell in cancer: towards marker and target identification. *Nat Rev Cancer* 2006;6: 835–45.
15. Taylor M, Rossler J, Geoerger B, Laplanche A, Hartmann O, Vassal G, Farace F. High levels of circulating VEGFR2+ Bone marrow-derived progenitor cells correlate with metastatic disease in patients with pediatric solid malignancies. *Clin Cancer Res* 2009;15:4561–71.
16. Wilmes LJ, Pallavicini MG, Fleming LM, Gibbs J, Wang D, Li KL, Partridge SC, Henry RG, Shalinsky DR, Hu-Lowe D, Park JW, McShane TM, et al. AG-013736, a novel inhibitor of VEGF receptor tyrosine kinases, inhibits breast cancer growth and decreases vascular permeability as detected by dynamic contrast-enhanced magnetic resonance imaging. *Magn Reson Imaging* 2007;25: 319–27.
17. Hu-Lowe DD, Zou HY, Grazzini ML, Hallin ME, Wickman GR, Amundson K, Chen JH, Rewolinski DA, Yamazaki S, Wu EY, McTigue MA, Murray BW, et al. Nonclinical antiangiogenesis and antitumor activities of axitinib (AG-013736), an oral, potent, and selective inhibitor of vascular endothelial growth factor receptor tyrosine kinases 1, 2, 3. *Clin Cancer Res* 2008;14: 7272–83.
18. Rixe O, Bukowski RM, Michaelson MD, Wilding G, Hudes GR, Bolte O, Motzer RJ, Bycott P, Liau KF, Freddo J, Trask PC, Kim S, et al. Axitinib treatment in patients with cytokine-refractory metastatic renal-cell cancer: a phase II study. *Lancet Oncol* 2007;8:975–84.
19. Cohen EE, Rosen LS, Vokes EE, Kies MS, Forastiere AA, Worden FP, Kane MA, Sherman E, Kim S, Bycott P, Tortorici M, Shalinsky DR, et al. Axitinib is an active treatment for all histologic subtypes of advanced thyroid cancer: results from a phase II study. *J Clin Oncol* 2008;26: 4708–13.
20. Schiller JH, Larson T, Ou SH, Limentani S, Sandler A, Vokes E, Kim S, Liau K, Bycott P, Olszanski AJ, von PJ. Efficacy and safety of axitinib in patients with advanced non-small-cell lung cancer: results from a phase II study. *J Clin Oncol* 2009;27:3836–41.
21. Hersey P, Bastholt L, Chiarion-Sileni V, Cinat G, Dummer R, Eggermont AM, Espinosa E, Hauschild A, Quirt I, Robert C, Schadendorf D. Small molecules and targeted therapies in distant metastatic disease. *Ann Oncol* 2009;20 (Suppl 6): vi35–40.
22. Choueiri TK. Axitinib, a novel anti-angiogenic drug with promising activity in various solid tumors. *Curr Opin Investig Drugs* 2008;9:658–71.
23. Ferrandis E, Da SJ, Riou G, Benard I. Coactivation of the MDR1 and MYCN genes in human neuroblastoma cells during the metastatic process in the nude mouse. *Cancer Res* 1994;54:2256–61.
24. Vassal G, Terrier-Lacombe MJ, Bissery MC, Venuat AM, Gyergyay F, Benard J, Morizet J, Boland I, Ardouin P, Bressac-de-Paillerets B, Gouyette A. Therapeutic activity of CPT-11, a DNA-topoisomerase I inhibitor, against peripheral primitive neuroectodermal tumour and neuroblastoma xenografts. *Br J Cancer* 1996;74:537–45.
25. Elie N, Plancoulaine B, Signolle JP, Herlin P. A simple way of quantifying immunostained cell nuclei on the whole histologic section. *Cytometry A* 2003;56: 37–45.
26. Ting N. Dose finding in drug development (Statistics for biology and health). New York: Springer; 2006.
27. Tesselaar E, Henricson J, Jonsson S, Sjoberg F. A time-response model for analysis of drug transport and blood flow response during iontophoresis of acetylcholine and sodium nitroprusside. *J Vasc Res* 2009;46:270–7.
28. Ma J, Waxman DJ. Dominant effect of antiangiogenesis in combination therapy involving cyclophosphamide and axitinib. *Clin Cancer Res* 2009;15:578–88.
29. Langer I, Vertongen P, Perret J, Fontaine J, Atassi G, Robberecht P. Expression of vascular endothelial growth factor (VEGF) and VEGF receptors in human neuroblastomas. *Med Pediatr Oncol* 2000; 34:386–93.
30. Beierle EA, Dai W, Langham MR, Jr, Copeland EM, III, Chen MK. Expression of VEGF receptors in cocultured neuroblastoma cells. *J Surg Res* 2004;119: 56–65.
31. Sims TL, Williams RF, Ng CY, Rosati SF, Spence Y, Davidoff AM. Bevacizumab

suppresses neuroblastoma progression in the setting of minimal disease. *Surgery* 2008;144:269–75.
32. Fukuzawa M, Sugiura H, Koshinaga T, Ikeda T, Hagiwara N, Sawada T. Expression of vascular endothelial growth factor and its receptor Flk-1 in human neuroblastoma using in situ hybridization. *J Pediatr Surg* 2002;37:1747–50.
33. Geoerger B, Brasme JF, Daudigeos-Dubus E, Opolon P, Venot C, Debussche L, Vrignaud P, Vassal G. Anti-insulin-like growth factor 1 receptor antibody EM164 (murine AVE1642) exhibits anti-tumour activity alone and in combination with temozolomide against neuroblastoma. *Eur J Cancer*. 2010 Jun 28. [Epub ahead of print].
34. Kurmasheva RT, Harwood FC, Houghton PJ. Differential regulation of vascular endothelial growth factor by Akt and mammalian target of rapamycin inhibitors in cell lines derived from childhood solid tumors. *Mol Cancer Ther* 2007;6: 1620–8.
35. Fenton BM, Paoni SF. The addition of AG-013736 to fractionated radiation improves tumor response without functionally normalizing the tumor vasculature. *Cancer Res* 2007;67:9921–8.
36. Rugo HS, Herbst RS, Liu G, Park JW, Kies MS, Steinfeldt HM, Pithavala YK, Reich SD, Freddo JL, Wilding G. Phase I trial of the oral antiangiogenesis agent AG-013736 in patients with advanced solid tumors: pharmacokinetic and clinical results. *J Clin Oncol* 2005;23:5474–83.
37. Shaked Y, Henke E, Roodhart JM, Mancuso P, Langenberg MH, Colleoni M, Daenen LG, Man S, Xu P, Emmenegger U, Tang T, Zhu Z, et al. Rapid chemotherapy-induced acute endothelial progenitor cell mobilization: implications for antiangiogenic drugs as chemosensitizing agents. *Cancer Cell* 2008;14: 263–73.
38. Rossler J, Lagodny J. Blood and lymph vessels in embryonic tumors. *Hematol Oncol* 2005;23:94–101.
39. Glade Bender JL, Adamson PC, Reid JM, Xu L, Baruchel S, Shaked Y, Kerbel RS, Cooney-Qualter EM, Stempak D, Chen HX, Nelson MD, Krailo MD, et al. Phase I trial and pharmacokinetic study of bevacizumab in pediatric patients with refractory solid tumors: a Children's Oncology Group Study. *J Clin Oncol* 2008; 26:399–405.